Journal of Zhejiang University-SCIENCE C (Computers & Electronics)
ISSN 1869-1951 (Print); ISSN 1869-196X (Online)
www.zju.edu.cn/jzus; www.springerlink.com
E-mail: jzus@zju.edu.cn

Numerical solution of potential flow equations with a predictor-corrector finite difference method

Zhi-qiang LUO

(*Department of System Science and Applied Mathematics, School of Science, Kunming University of Science and Technology, Kunming 650083, China*)

E-mail: zql1009@126.com

Received Oct. 26, 2011; Revision accepted Feb. 9, 2012; Crosschecked Apr. 9, 2012

Abstract: We develop a numerical solution algorithm of the nonlinear potential flow equations with the nonlinear free surface boundary condition. A finite difference method with a predictor-corrector method is applied to solve the nonlinear potential flow equations in a two-dimensional (2D) tank. The irregular tank is mapped onto a fixed square domain with rectangular cells through a proper mapping function. A staggered mesh system is adopted in a 2D tank to capture the wave elevation of the transient fluid. The finite difference method with a predictor-corrector scheme is applied to discretize the nonlinear dynamic boundary condition and nonlinear kinematic boundary condition. We present the numerical results of wave elevations from small to large amplitude waves with free oscillation motion, and the numerical solutions of wave elevation with horizontal excited motion. The beating period and the nonlinear phenomenon are very clear. The numerical solutions agree well with the analytical solutions and previously published results.

Key words: Predictor-corrector method, Nonlinear potential flow equations, Finite difference method, Staggered grid, Nested iterative method

doi:10.1631/jzus.C1100313 **Document code:** A **CLC number:** O24

1 Introduction

The formulation of the potential flow problem with a free surface boundary condition was first developed by Friedrichs (1934), who used a variational principle to obtain the pressure condition on the free surface in steady flows. Luke (1967) gave a simple extension of this variational principle which arose from Whitham (1965). Shortly thereafter, a Hamiltonian formulation of the irrotational problem was introduced by Zakharov (1968) and later pursued by Miles (1977). The variational principles (Rocca *et al.*, 1997) can be used to construct solutions analytically, for numerical computations, or to analyze the stability of the formulae.

Several numerical schemes have been proposed to solve nonlinear potential flow equations with a free surface boundary condition in a two-dimensional (2D) tank. Penney and Price (1952) developed a successive approximation to the solution of the potential flow equations and carried the solution to the fifth order for the case of 2D wave on a deep liquid. Abramson (1966) presented theoretical and experimental results pertaining to undamped potential flow behavior in rigid containers and gave different analytical formulae of the potential functions. An important method was proposed by Moiseyev (1958), who developed a small perturbation parameter as a power series for velocity potential and wave elevation of free surface. Faltinsen (1974) applied this perturbation method to solve the potential flow equations and extended the nonlinear solution to third-order approximation. Faltinsen (1978) and Faltinsen and Timokha (2002) creatively built an asymptotic modal method of nonlinear potential flow, and the

revised modal equations took full account of nonlinearities up to fourth-order polynomial terms in generalized coordinates. Frandsen (2004) developed a fully nonlinear finite difference model based on inviscid potential flow equations. Ikegawa (1974) applied the finite element method to solve the potential flow problem and first analyzed the nonlinear water wave in a tank subjected to horizontal excitation. Nakayama and Washizu (1981) dealt with an application of the boundary element method (BEM) to the analyses of nonlinear potential flow problems. Hromadka and Whitley (2005) developed approximating three-dimensional (3D) steady state potential flow problems using 2D complex polynomials.

The current numerical methods for potential flow equations are listed in the following statements. Tarafder and Suzuki (2008) developed a numerical method of potential flow with free surface around a ship using the modified Rankine source panel method. Chainais-Hillairet *et al.* (2009) presented numerical solutions of Euler-Poisson systems for potential flows from a numerical viewpoint. Šarler (2009) expressed the solution of a 2D bubble shape in potential flow by the method of fundamental solutions. Wang and Zhang (2007) extended the numerical solution of potential flow from 2D to 3D space for the potential flow problem coupled with the dynamics of rigid body, which was developed to determine numerically the resultant force and moment of force acting on an arbitrary 3D solid body. Klaseboer *et al.* (2011) gave boundary element simulations of potential flow with viscous effects as applied to a rising bubble. Abbaspour and Hassanabad (2009) developed a novel 2D BEM with composed elements to study the sloshing phenomenon. Wu and Chen (2009) developed a time-independent finite difference method with a Crank-Nicolson scheme for inviscid and incompressible fluid.

Based on the above analyses, we propose a new difference method model for calculation of the nonlinear potential flow equations. For inviscid and incompressible fluid, we develop a finite difference method with a predictor-corrector scheme and design an iterative algorithm to solve the nonlinear potential flow equations. The finite difference method with a predictor-corrector scheme can be used to calculate the velocity potential and the wave elevation on the free surface. A nested iterative algorithm is applied to implement the complicated flow field. The time-varying fluid field is mapped onto a fixed square domain through proper σ coordinate transformation functions, and a staggered grid system is applied to capture the variables of the fluid field, such as the velocity potential ϕ, velocity components u, v, and the wave elevation h of the free surface. The wave elevation error values are presented with free oscillation motion and horizontal excited motion.

2 Mathematical formulation

In this section, we introduce the potential flow equations with free surface in a 2D tank. The potential flow Eqs. (1)–(7) are written based on the coordinate system in Fig. 1. The Cartesian coordinate system (xOy) is connected to the tank center with origin on the free surface, y pointing in the upward direction and x pointing in the horizontal right direction.

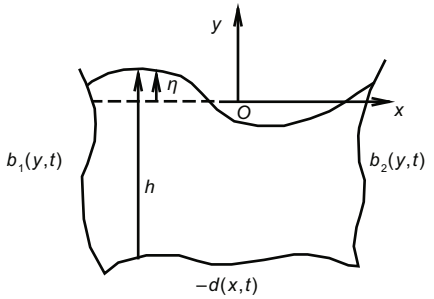

Fig. 1 Physical domain

In Fig. 1, the boundary on the base wall is denoted as $-d(x,t)$, which is a single valued function. The values of $b_1 = b_1(y,t)$ and $b_2 = b_2(y,t)$, which are single valued functions, are horizontal displacements measured from the y axis to the left wall and right wall respectively, and $h(x,t)$ is a single-valued function measured from the tank bottom to the free surface, $h = d + \eta$.

In the following fluid model, we assume the fluid is incompressible, irrotational, and inviscid. Following Luke's variational principle, the potential flow equations are derived and written as

$$\frac{\partial \phi}{\partial t} + \frac{1}{2}|\nabla \phi|^2 + (g + a_y(t))\, y + x a_x(t) + \frac{p - p_0}{\rho} = 0, \tag{1}$$

$$\Delta \phi = 0, \tag{2}$$

where ρ is the density of water, $a_x(t)$ the horizontal excited acceleration, $a_y(t)$ the vertical excited acceleration, p the pressure, p_0 the pressure on the free surface, ϕ the velocity potential, and g the gravity acceleration.

On the free surface the dynamic and kinematic boundary conditions hold, which are

$$\left[\frac{\partial\phi}{\partial t}+\frac{1}{2}|\nabla\phi|^2+(g+a_y(t))\,\eta+xa_x(t)\right]_{y=\eta}=0 \tag{3}$$

and

$$\left[\frac{\partial\eta}{\partial t}+\nabla\phi\cdot\nabla\eta-\frac{\partial\eta}{\partial y}\right]_{y=\eta}=0. \tag{4}$$

In the coordinate system fixed to the tank, the fluid velocity components normal to the fixed boundaries are equal to zero. Hence, on the bottom and the walls of the tank we have

$$\left.\frac{\partial\phi}{\partial x}\right|_{x=b_1,x=b_2}=0,\ \left.\frac{\partial\phi}{\partial y}\right|_{y=-d}=0. \tag{5}$$

The velocity components u and v are defined as

$$\frac{\partial\phi}{\partial x}=u,\ \frac{\partial\phi}{\partial y}=v. \tag{6}$$

Initially the fluid is assumed to be at rest with some initial perturbation of the free surface. Thus, the initial conditions are

$$\phi=0,\ \eta=\eta_0,\ t=0. \tag{7}$$

3 Coordinate transformation and non-dimensionalization of potential flow equations

3.1 Coordinate transformation

A physical domain in Fig. 1 can be transformed to a regular square tank with rectangular cells in Fig. 2 by a proper coordinate transformation described by Eqs. (8) and (9), which is a σ coordinate transformation (Phillips, 1957). In the physical domain, the grid size is (M,N), and $b_1=x_1\leq x_2\leq\cdots\leq x_{M+1}=b_2$, $-d=y_1\leq y_2\leq\cdots\leq y_{N+1}=\eta$.

The formulae of the coordinate transformation are

$$X=\frac{x-b_1}{b_2-b_1} \tag{8}$$

and

$$Y=\frac{y+d}{h}. \tag{9}$$

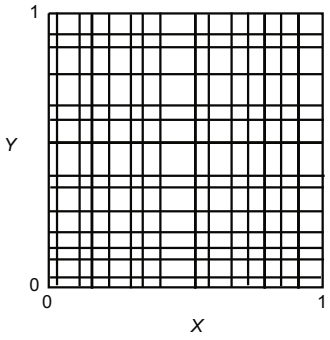

Fig. 2 Transformation domain

3.2 Non-dimensionalization of potential flow equations

To show the dimensionless treatment of potential flow equations in the physical domain, we give some characteristic parameters. The variables in the physical domain, including the velocity potential ϕ, the elevation h, the pressure p, the time t, the coordinates x, y, and the velocity components u, v, are normalized in the following ways:

$$\begin{aligned}&\Phi=\frac{\phi}{d_0\sqrt{gd_0}},H=\frac{h}{d_0},P=\frac{p}{\rho gd_0},T=\frac{t\sqrt{gd_0}}{d_0},\\&X_1=\frac{x}{d_0},Y_1=\frac{y}{d_0},U=\frac{u}{\sqrt{gd_0}},V=\frac{v}{\sqrt{gd_0}},\end{aligned} \tag{10}$$

where d_0 is the distance measured vertically from the base wall to the still free surface, and the dimensionless accelerations are denoted as

$$X_{\rm a}=\frac{a_x(t)}{g},Y_{\rm a}=\frac{a_y(t)}{g}. \tag{11}$$

With the formulae of coordinate transformations and dimensionless variables, Eqs. (1)–(7) can be written in the following dimensionless forms:

$$\begin{aligned}&\Phi_T+c_5\Phi_X+c_6\Phi_Y+\frac{1}{2}\Big[(c_1\Phi_X+c_2\Phi_Y)^2+(c_3\Phi_X\\&+c_4\Phi_Y)^2\Big]+(1+Y_{\rm a})Y_1+X_1X_{\rm a}+(P-P_0)=0,\end{aligned} \tag{12}$$

$$\begin{aligned}&\Phi_T+c_5\Phi_X+c_6\Phi_Y+\frac{1}{2}\Big[(c_1\Phi_X+c_2\Phi_Y)^2+(c_3\Phi_X\\&+c_4\Phi_Y)^2\Big]+(1+Y_{\rm a})(H-1)+X_1X_{\rm a}|_{y=h-d}=0,\end{aligned} \tag{13}$$

$$\begin{aligned}&[H_T+c_5H_X+c_6H_Y+U(c_1H_X+c_2H_Y)\\&-V]_{y=h-d}=0,\end{aligned} \tag{14}$$

$$\sqrt{\frac{g}{d_0}}\Big[(c_1^2+c_3^2)\Phi_{XX}+2(c_1c_2+c_3c_4)\Phi_{XY} +(c_2^2+c_4^2)\Phi_{YY}\Big]=0, \quad (15)$$

$$\begin{cases}\sqrt{gd_0}\,(c_1\Phi_X+c_2\Phi_Y)|_{X=0,1}=0,\\ \sqrt{gd_0}\,(c_3\Phi_X+c_4\Phi_Y)|_{Y=0}=0,\end{cases} \quad (16)$$

$$U=c_1\Phi_X+c_2\Phi_Y, V=c_3\Phi_X+c_4\Phi_Y, \quad (17)$$

$$\Phi=0, H=H_0, T=0. \quad (18)$$

Φ_T is the derivative of Φ with respect to the dimensionless time T, and the other derivatives are similarly defined. The coefficients $c_1, c_2, \cdots, c_6$ are the parameters resulting from the coordinate transformations. These coefficients are listed in the following schemes:

$$c_1=d_0\frac{\partial X}{\partial x}, \quad (19)$$

$$c_2=d_0\frac{\partial Y}{\partial x}, \quad (20)$$

$$c_3=d_0\frac{\partial X}{\partial y}, \quad (21)$$

$$c_4=d_0\frac{\partial Y}{\partial y}, \quad (22)$$

$$c_5=\frac{d_0}{\sqrt{gd_0}}\frac{\partial X}{\partial t}, \quad (23)$$

$$c_6=\frac{d_0}{\sqrt{gd_0}}\frac{\partial Y}{\partial t}. \quad (24)$$

4 Finite difference method with a predictor-corrector scheme for potential flow equations

In this section, a very effective finite difference technique is shown for inviscid, irrotational, and incompressible flow. To find the solution, a staggered grid system is used to analyze the fluid field in a square tank in Fig. 2 with rectangular cells in Fig. 3. From Fig. 3, the velocity potential Φ and velocity components U, V are defined in a rectangular cell. For the time T=$n\Delta T$, the velocity potential $\Phi_{i,j}^n$ is defined at the center (X_i, Y_j) of a cell. The velocity components $U_{i,j}^n$ and $V_{i,j}^n$ are calculated at $0.5\Delta X_i$ behind the cell center (X_i, Y_j) and at $0.5\Delta Y_j$ below the cell center (X_i, Y_j).

The predictor-corrector scheme is used to calculate the velocity potential of the dynamic boundary condition on the free surface and to solve the elevation H, with respect to the kinematic boundary condition for $T=n\Delta T$ and at the nodes (X_i, Y_j). All terms at the left-hand side of Eqs. (12)–(18) are discretized at the same nodes (X_i, Y_j) and for the same time $T=n\Delta T$. To apply the predictor-corrector scheme, the dimensionless Eqs. (13) and (14) are arranged as in the following schemes:

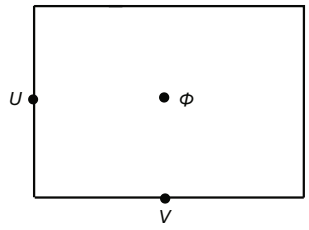

Fig. 3 Staggered grid cell

$$\frac{\partial\Phi}{\partial T}=-\Big\{c_5\Phi_X+c_6\Phi_Y+\frac{1}{2}\big[(c_1\Phi_X+c_2\Phi_Y)^2+(c_3\Phi_X+c_4\Phi_Y)^2\big]+(1+Y_a)(H-1)+X_1X_a\Big\}, \quad (25)$$

$$\frac{\partial H}{\partial T}=-\left[c_5H_X+c_6H_Y+U(c_1H_X+c_2H_Y)-V\right]. \quad (26)$$

4.1 Predictor stage

At the first predictor stage, the intermediate solutions $(\Phi_{i,j}^*)^{n+1}$ and $(H_{i,j}^*)^{n+1}$ are calculated from Eqs. (27)–(29):

$$(\Phi_{i,j}^*)^{n+1}=\Phi_{i,j}^n-\Delta T\Big\{c_5\Phi_X+c_6\Phi_Y+\frac{1}{2}\big[(c_1\Phi_X+c_2\Phi_Y)^2+(c_3\Phi_X+c_4\Phi_Y)^2\big]+(1+Y_a)(H-1)+X_1X_a\Big\}\Big|_{i,j}^n, \quad (27)$$

$$\begin{cases}(U_{i,j}{}^*)^{n+1}=(c_1\Phi_X^*+c_2\Phi_Y^*)|_{i,j}^{n+1},\\ (V_{i,j}{}^*)^{n+1}=(c_3\Phi_X^*+c_4\Phi_Y^*])|_{i,j}^{n+1},\end{cases} \quad (28)$$

$$(H_{i,j}^*)^{n+1}=H_{i,j}^n-\Delta T\big[c_5H_X+c_6H_Y+U(c_1H_X+c_2H_Y)-V\big]\big|_{i,j}^n. \quad (29)$$

The schemes are constructed from forward difference formulae in space (i, j) and in time $n\Delta T$.

4.2 Corrector stage

The corrector values of the elevation H and the velocity potential Φ are calculated with the following schemes:

$$\begin{cases} \Phi^{**} = \dfrac{(\Phi^{*}_{i,j})^{n+1} + (\Phi_{i,j})^{n}}{2}, \\ U^{**} = \dfrac{(U^{*}_{i,j})^{n+1} + (U_{i,j})^{n}}{2}, \\ V^{**} = \dfrac{(V^{*}_{i,j})^{n+1} + (V_{i,j})^{n}}{2}, \\ H^{**} = \dfrac{(H^{*}_{i,j})^{n+1} + (H_{i,j})^{n}}{2}, \end{cases} \tag{30}$$

$$\begin{aligned} \Phi^{n+1}_{i,j} =& \Phi^{n}_{i,j} - \Delta T\Big\{c_5\Phi^{**}_X + c_6\Phi^{**}_Y + \frac{1}{2}\big[(c_1\Phi^{**}_X \\ &+ c_2\Phi^{**}_Y)^2 + (c_3\Phi^{**}_X + c_4\Phi^{**}_Y)^2\big] \\ &+ (1+Y_{\mathrm{a}})(H^{**}-1) + X_1X_{\mathrm{a}}\Big\}, \end{aligned} \tag{31}$$

$$\begin{aligned} H^{n+1}_{i,j} =& H^{n}_{i,j} - \Delta T\Big[c_5H^{**}_X + c_6H^{**}_Y + U^{**}(c_1H^{**}_X \\ &+ c_2H^{**}_Y) - V^{**}\Big]. \end{aligned} \tag{32}$$

The point successive over the relaxation method is used to calculate the velocity potential Eq. (15). We give the following iterative scheme:

$$\begin{aligned} \Phi^{n+1}_{i,j} =& \Phi^{n}_{i,j} - \frac{\omega}{a_{i,j}}\Big[(c_1^2+c_3^2)\Phi^{**}_{XX} + 2(c_1c_2 \\ &+ c_3c_4)\Phi^{**}_{XY} + (c_2^2+c_4^2)\Phi^{**}_{YY}\Big], \end{aligned} \tag{33}$$

where ω is a constant factor and $0<\omega<2$, and $a_{i,j}$ is the sum of the coefficients of the velocity potential $\Phi_{i,j}$.

5 Approximate von Neumann stability condition

To derive the stability condition, a physical domain with a non-homogeneous mesh is divided by $b_1 = x_1 \le x_2 \le \cdots \le x_{M+1} = b_2$, $-d = y_1 \le y_2 \le \cdots \le y_{N+1} = \eta$. The mesh grid number is (M, N).

We shall consider the linearized potential flow equation on the interval $[b_1, b_2] \times [-d, \eta]$:

$$\left[\phi_t + \frac{1}{2}(u\phi_x + v\phi_y) + \big(g + a_y(t)\big)\eta\right]_{y=\eta} = 0, \tag{34}$$

where u and v are constant velocity components.

The solution ϕ is discretized by $\phi^n_{i,j}$, a backward difference scheme for $\frac{\partial\phi}{\partial x}$ and $\frac{\partial\phi}{\partial y}$. Eq. (34) is then discretized by

$$\begin{aligned} \phi_t\big|^{n+1/2}_{i,j} + \frac{1}{2}\,(u\phi_x + v\phi_y)\big|^{n+1/2}_{i,j} + \big(g + a_y(t)\big)\eta\big|^{n+1/2}_{i,j} \\ = 0. \end{aligned} \tag{35}$$

We set $\phi(x,y,t_n) = G(k,l)\mathrm{e}^{i(k,l)\cdot(x,y)} = G(k,l)\mathrm{e}^{ikx}\mathrm{e}^{ily}$. We consider a small amplitude wave for which Eq. (35) can be denoted by

$$\begin{aligned} \frac{G(k,l)-1}{\Delta t} + \frac{1}{2}\Bigg(\bar{u}\frac{G\mathrm{e}^{ik\Delta x} - G + \mathrm{e}^{-ik\Delta x} - 1}{2\Delta x} \\ + \bar{v}\frac{G\mathrm{e}^{il\Delta y} - G + e^{-il\Delta y} - 1}{2\Delta y}\Bigg) = 0. \end{aligned} \tag{36}$$

The growth factor $G(k,l)$ satisfies $|G(k,l)| < 1$, so the difference scheme (36) is unconditionally stable. The stability criterion is restricted with

$$\Delta t\left(\frac{|u|}{4\Delta x} + \frac{|v|}{4\Delta \mathrm{y}}\right) < 1. \tag{37}$$

6 Iterative algorithm for potential flow equations

The iterative procedure of the finite difference method for potential flow equations is given below. The first step is to obtain the velocity potential Φ through solving the Poisson equation. Then substituting the results into the derivatives of the velocity potential, we can obtain the velocity components U and V. Further substituting the velocity components into the kinematic boundary condition, the elevation H on the free surface can be solved. The dynamic and kinematic boundary equations on the free surface can be solved with the similar Crank-Nicolson scheme. The convergence criteria for nested iteration of Φ and H are set as $||\Phi^{k+1} - \Phi^k||_\infty < 10^{-7}$ and $||H^{k+1} - H^k||_\infty < 10^{-7}$, where k is an iterative number.

This iterative algorithm for the time $T = (n + 1/2)\Delta T$ and the spatial position (X_i, Y_j) is written in the following process in detail:

1. Give initial values Φ and H.
2. Calculate velocity potential Φ from Eq. (33).
3. Calculate the free surface H from Eq. (32), and check the convergence criterion of H. If the convergence criterion is not satisfied, go to step 2.

4. If Φ and H converge, proceed to the next time step.

7 Numerical results

In this section, the proposed finite difference schemes for 2D potential flow equations are compared with the analytical solutions. We present free oscillation motion and horizontal excited motion. To verify the precision of numerical solutions, we calculate the error values between the numerical solutions and analytical solutions. The numerical results are compared with the analytical results and the previously published results.

To calculate the numerical solution, a rectangular fluid tank is given. b_2-b_1 is the width of the tank, d_0 denotes the still water depth, $d=d_0$, and the natural circular frequency is $\omega_n=\sqrt{gk_n\tanh(k_nd_0)}$, where $k_n=n\pi/(b_2-b_1), n=1,2,\cdots$. The surge motion is given as $X_c=-X_0\omega_x^2\cos(\omega t)$, the initial wave is $Y=A\cos(k_nx)$, A is the initial wave amplitude, $M\times N$ is the mesh grid number, and the time step is $\Delta t=0.001$ s.

7.1 Free oscillation motion

In this subsection, we present the free oscillation motion. The tank width is (b_2-b_1) m, and the tank depth is set as d m. We consider a typical standing wave problem described by a cosine wave $A\cos(\pi x)$. For this case, the second-order analytical solution (Frandsen, 2004) for this problem is

$$h(x,t)=d+A\cos(\omega_nt)\cos(k_nx)+\frac{A\omega_n^2}{g}\left[\frac{1}{8}\left(1+\frac{g^2k_n^2}{\omega_n^4}\right)+\left(\frac{1}{8}\frac{3\omega_n^4-g^2k_n^2}{\omega_n^4}-\frac{3}{2}\frac{\omega_n^4-g^2k_n^2}{\omega_n^2(4\omega_n^2-\omega_{2n}^2)}\right)\cos(2\omega_nt)+\frac{1}{2}\frac{\omega_n^2\omega_{2n}^4-\omega_n^4-3g^2k_n^2}{\omega_n^2(4\omega_n^2-\omega_{2n}^2)}\cos(\omega_{2n}t)\right]\cos(2k_nx), \tag{38}$$

where $\omega_{2n}=\sqrt{2gk_n\tanh(2k_nd_0)}$.

We first calculate the wave elevation error values between numerical and analytical solutions. The tank width and tank depth are set at $b_2-b_1=1.0$ m and $d=0.5$ m, respectively, an initial cosine wave with wave length $\lambda=2$ m, and the amplitude $A=0.002$ m.

The error values of the wave elevation on the free surface are calculated (Table 1). The numerical solution H^{numer} and the analytical solutions $H^{\mathbf{anal}}$ with respect to different mesh numbers (M,N) at the horizontal positions $x_1=b_1$, $x_2=b_2$, and $x_3=(b_1+b_2)/2$ on the free surface are listed in 5 s.

The wave elevation error values between numerical and analytical solutions are very small; therefore, the finite difference method for potential flow equations is very effective. The impact of the mesh grid number for free oscillation is very small.

In the following calculations, the numerical solutions of wave elevation with free oscillation are calculated. The tank width and tank depth are set as $b_2-b_1=1.0$ m and $d=0.5$ m, respectively, $\Delta t=0.001$ s, and an initial cosine wave with wave length $\lambda=2$ m.

We provide numerical experiment results based on the present method for the initial wave amplitude A=0.002 m. From Fig. 4, the time history of the wave elevation in 10 s is plotted and the numerical solution agrees well with the analytical solution on the free surface at the left wall.

We increase the amplitude to the value $A=0.02$ m. In Fig. 5, the numerical solution and analytical solution (Frandsen, 2004) on the free surface at the left wall are calculated and plotted. The numerical solution agrees well with the analytical solution.

We increase the amplitude to the value $A=0.1$ m and present the numerical results of the wave elevations at the left wall for the large amplitude wave (Fig. 6). The numerical solution does not match the analytical solution closely for $A=0.1$ m. With respect to the analytical solution of the exact solution, the second-order analytical solution is not suitable for the large amplitude wave. Fig. 6 shows that the errors are still small. For the large amplitude wave, the numerical results are still very

Table 1 The wave elevation error values between the numerical solutions and analytical solutions

Mesh grid (M,N)	$\|\|H_{x_1}^{\text{anal}}-H_{x_1}^{\text{numer}}\|\|_\infty$	$\|\|H_{x_2}^{\text{anal}}-H_{x_2}^{\text{numer}}\|\|_\infty$	$\|\|H_{x_3}^{\text{anal}}-H_{x_3}^{\text{numer}}\|\|_\infty$
$(50,20)$	2.0853e-005	1.8532e-005	1.1374e-006
$(60,40)$	5.5402e-005	5.1716e-005	1.6473e-006

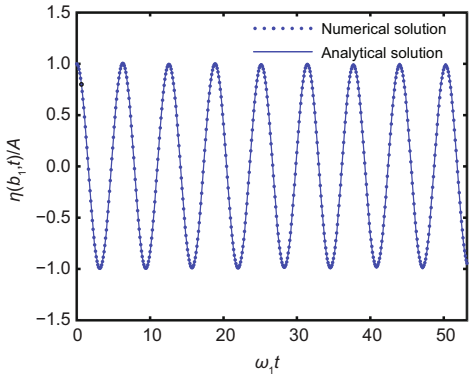

Fig. 4 The wave elevations of the standing wave on the free surface at the left wall $x = b_1$ (amplitude A=0.002 m)

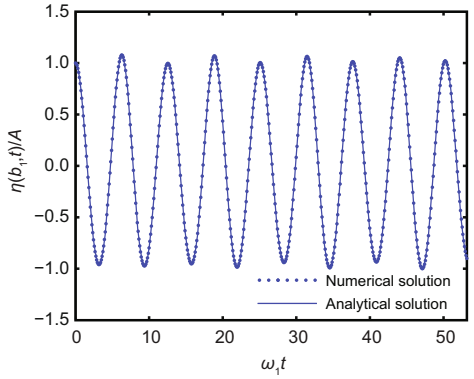

Fig. 5 The wave elevation of the free surface at the left wall (initial wave amplitude $A = 0.02$ m)

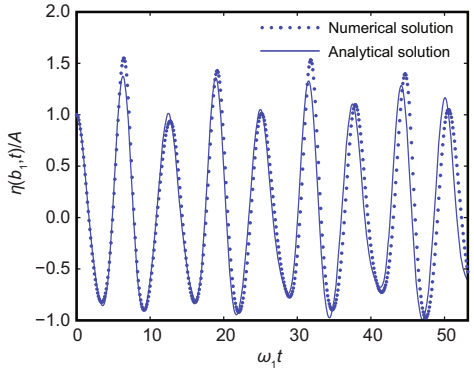

Fig. 6 The wave elevation of the free surface at the left wall (the amplitude $A = 0.1$ m)

good.

To present the numerical effects with the present finite difference method, we give numerical solutions of the potential flow equations and compare these numerical solutions with that in Frandsen (2004). The parameters are $b_2 - b_1 = 1.0$ m, $d = 0.5$ m, the grid size $(M, N) = (50, 20)$. We list the present work in Fig. 7b and compare this work with Frandsen (2004) in Fig. 7a. The present work agrees with Frandsen (2004) for which the wave steepness is $\varepsilon = 0.00144, 0.144$, or 0.288, where ε is defined as $A\omega_n^2/g$.

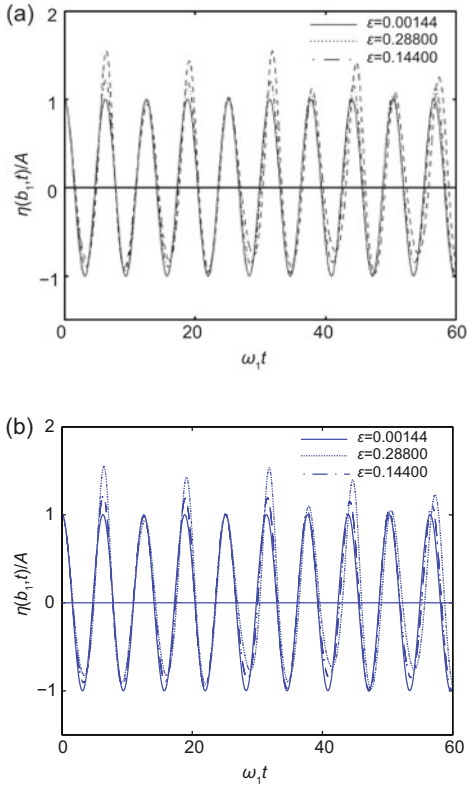

Fig. 7 The wave elevation of the free surface at the left wall. (a) Frandsen's work; (b) Finite difference method

7.2 Horizontal excited motion

The tank width and tank depth are set at $b_2 - b_1$ and d, respectively. The potential flow equations are loaded with a horizontal acceleration $X_a(t) = -X_0\omega^2\cos(\omega t)$. For this problem, the first-order analytical solution (Wu, 2007) is written as

$$\begin{cases} \phi^{(1)} = \sum_{n=1}^{\infty} A_n(t)\dfrac{\cosh\left(k_n(y+d)\right)}{\cosh(k_n d)}\cos\left(k_n(x+a)\right), \\ \eta^{(1)} = d + \dfrac{1}{g}\sum_{n=1}^{\infty}\dot{A}_n(t)\cos\left(k_n(x+a)\right), \end{cases} \tag{39}$$

where the parameters $A_n = -[(-1)^n - 1]/(k_n^2 a) \times\omega_n \int_0^t \dot{r_x}(s)\sin(\omega_n(t-s))\mathrm{d}s$, k_n is the wave number, $\omega_n{=}\sqrt{gk_n\tanh(k_n d)}$, $r_x(t){=}{-}X_0\omega\sin(\omega t)$, $a{=}(b_2 - b_1)/2$.

For the horizontal excited motion, we first calculate the wave elevation error values between numerical and analytical solutions. The tank width and tank depth are set at $b_2 - b_1 = 1.0$ m and $d = 0.5$ m, respectively. The excited acceleration is $X_a(t) = -X_0\omega^2\cos(\omega t)$, $\omega = 0.9\omega_1$, $X_0 = 0.002$ m. The wave elevation errors between numerical and analytical solutions are listed in Table 2.

Table 2 lists the wave elevation errors on the free surface at the left wall, right wall, and mean free surface. The wave elevation errors between numerical and analytical solutions are very small in the 5 s interval. It is clear that the errors decrease with the increase of the mesh grid number. Table 2 shows that the numerical solutions of horizontal excited motion with the finite difference method is very effective.

We give a numerical test for a horizontal excited motion in a 2D tank. We choose these parameters $b_2 - b_1 = 0.9$ m, $d = 0.6$ m, $\Delta t = 0.001$ s, $X_a = X_0\omega^2\sin(\omega t)$, $\omega = 5.5$ rad/s, $X_0 = 0.002$ m.

In Fig. 8, we plot the numerical solution and compare this solution with the previously published result based on the boundary element method (Nakayama and Washizu, 1981). The numerical solution in the present method agrees well with that of the boundary element method.

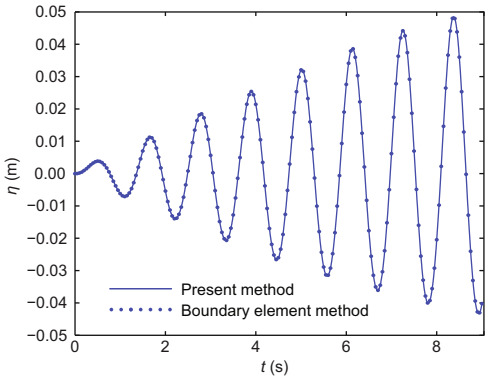

Fig. 8 The wave elevations on the free surface at the right wall $x = b_2$ in 9 s

In the following horizontal excited tests, the numerical solutions of potential flow equations are presented and the numerical solutions are compared with the analytical solutions (Wu, 2007). We consider the following computation parameters with respect to $b_2 - b_1 = 1.0$ m, $d = 0.5$ m, and $\Delta t = 0.001$ s in a 2D rectangular tank. The horizontal force with acceleration $X_a = -X_0\omega^2\cos(\omega t)$, $X_0 = 0.002$ m. In Fig. 9a, we choose the excited frequency $\omega = 0.7\omega_1$ and give the numerical solution and analytical solution. Fig. 9a shows that the numerical solution agrees well with the analytical solution. From Fig. 9b, we choose the frequency $\omega = 0.95\omega_1$ and present the numerical solution and analytical solution. Fig. 9b shows that the numerical solution agrees well with the analytical solution.

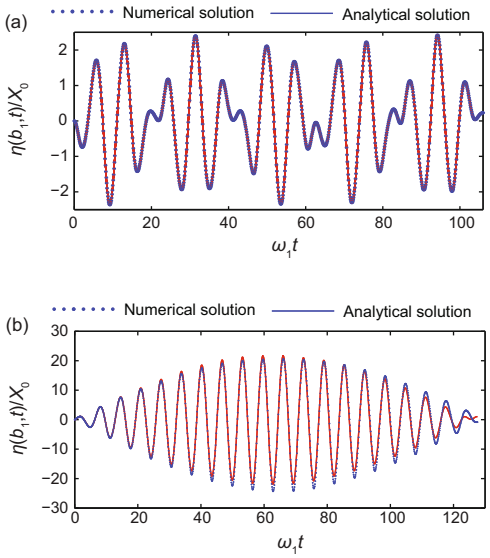

Fig. 9 The wave elevations on the free surface at the left wall $x = b_1$. (a) $\omega = 0.7\omega_1$, $t = 20$ s; (b) $\omega = 0.95\omega_1$, $t = 24$ s

Finally, two examples are given to implement the long time history motion with horizontal excited acceleration. In Fig. 10, we present the long time history wave elevation in 70 s. The param-

Table 2 The wave elevation error values between the numerical solutions of horizontal excitation motion and analytical solutions in 5 s with different mesh parameters (M, N)

Mesh grid (M, N)	$\|\|H_{x_1}^{\text{anal}} - H_{x_1}^{\text{numer}}\|\|_\infty$	$\|\|H_{x_2}^{\text{anal}} - H_{x_2}^{\text{numer}}\|\|_\infty$	$\|\|H_{x_3}^{\text{anal}} - H_{x_3}^{\text{numer}}\|\|_\infty$
$(50, 20)$	9.146e-004	7.939e-004	6.845e-004
$(60, 40)$	8.236e-004	7.672e-004	6.637e-004

eters are $X_a = -X_0\omega^2\cos(\omega t)$, $b_2 - b_1 = 1.0$ m, $d = 0.5$ m, $X_0 = 0.002$ m, $\omega = 1.03\omega_1$ and $\omega = 0.95\omega_1$. In Fig. 11, we present the long time history wave elevation in 36 s. The parameters are $X_a = -X_0\omega^2\cos(\omega t)$, $b_2 - b_1 = 0.9$ m, $d = 0.6$ m, $X_0 = 0.002$ m, and $\omega = 0.95\omega_1$. From Figs. 10 and 11, the beating phenomenon and nonlinear phenomenon are very clear.

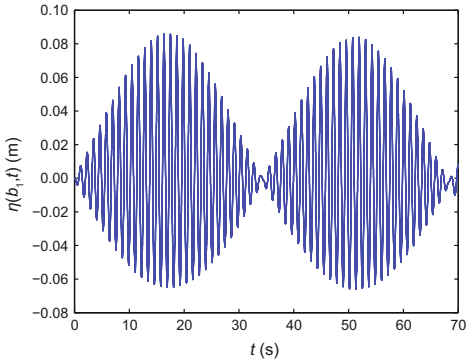

Fig. 10 The long time history of elevations at the left wall on the free surface in 70 s (Δt =0.001 s)

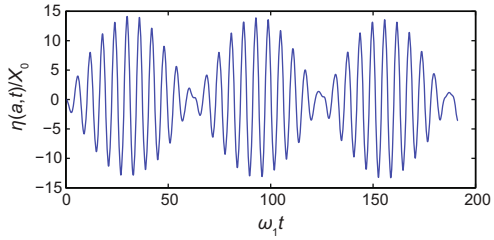

Fig. 11 The long time history of wave elevation at the left wall on the free surface in 36 s (Δt =0.001 s)

8 Conclusions

A finite difference method for potential flow equations is used to study the wave elevation of the free surface with a σ coordinate transformation in a 2D tank. A staggered grid system is applied to the computational domain and a coupling iterative method is used to solve the variables of the flow field, such as the velocity components U and V, the velocity potential Φ, and the wave elevation H.

We calculate the numerical solutions of the wave elevations for free oscillation motion and compare them with the second-order analytical solution (Frandsen, 2004). We also calculate the numerical solution of the wave elevation for horizontal excited motion and compare it with the first-order analytical solution (Wu, 2007). From the results, the numerical solutions agree with the analytical solutions. We give the wave elevation error values between the numerical and analytical solutions for horizontal excited motion and free oscillation motion. The numerical results show that the numerical solutions agree well with the analytical solutions for small amplitude wave with horizontal and free oscillation. For large amplitude wave, the numerical solution does not agree with the analytical solution, but the error values are still small. For free oscillation and horizontal excited oscillation, the numerical solutions agree well with those of Frandsen (2004) and Nakayama and Washizu (1981). We can conclude that the present finite difference method is very effective. To increase the accuracy of the numerical solution, the dynamic boundary condition would be discretized by the second-order Adams-Bashforth scheme.

Future research directions include (1) applying the 2D algorithms developed in this paper to numerical applications (such as the dynamic behavior of dam and circular tank) and (2) developing a 3D finite difference scheme, which has been developed and can be used to simulate the standing wave and solidity wave.

References

Abbaspour, M., Hassanabad, M.G., 2009. A novel 2D BEM with composed elements to study sloshing phenomenon. *J. Appl. Fluid Mech.*, **2**(2):77-83.

Abramson, H.N., 1966. The Dynamic Behavior of Liquids in Moving Containers. Technical Report, SP 106. NASA.

Chainais-Hillairet, C., Peng, Y.J., Violet, I., 2009. Numerical solutions of Euler–Poisson systems for potential flows. *Appl. Numer. Math.*, **59**(2):301-315.

Faltinsen, O.M., 1974. A nonliner theory of sloshing in retangular tanks. *J. Ship Res.*, **18**(4):224-241.

Faltinsen, O.M., 1978. A numerical non-linear method of sloshing in tanks with two dimensional flow. *J. Ship Res.*, **18**(4):224-241.

Faltinsen, O.M., Timokha, A.N., 2002. Asymptotic modal approximation of nonlinear resonant sloshing in a rectangular tank with small fluid depth. *J. Fluid Mech.*, **470**:319-357. [doi:10.1017/S0022112002002112]

Frandsen, J.B., 2004. Sloshing motions in excited tanks. *J. Comput. Phys.*, **196**(1):53-87. [doi:10.1016/j.jcp.2003.10.031]

Friedrichs, K., 1934. Über ein minimumproblem für potentialströmungen mit freiem rande. *Math. Ann.*, **109**(1):60-82 (in French). [doi:10.1007/BF01449125]

Hromadka, T.V., Whitley, R.J., 2005. Approximating three-dimensional steady-state potential flow problems using two-dimensional complex polynomials. *Eng. Anal.*

Bound. Elem., **29**(2):190-194. [doi:10.1016/j.enganabound.2004.07.004]

Ikegawa, M., 1974. Finite Element Analysis of Fluid Motion in a Container, Infinite Element Methods in Flow Problems. UAH Press, Huntsville.

Klaseboer, E., Derek, R.M., Chan, Y.C., 2011. BEM simulations of potential flow with viscous effects as applied to a rising bubble. *Eng. Anal. Bound. Elem.*, **35**(3):489-494. [doi:10.1016/j.enganabound.2010.09.005]

Luke, J.C., 1967. A variational principle for a fluid with a free surface. *J. Fluid Mech.*, **27**(2):395-397. [doi:10.1017/S0022112067000412]

Miles, J.W., 1977. On Hamilton's principle for surface waves. *J. Fluid Mech.*, **83**(1):153-158. [doi:10.1017/S0022112077001104]

Moiseyev, N.N., 1958. On the theory of nonlinear vibrations of a liquid of finite volume. *Appl. Math. Mech.*, **22**(5):224-241.

Nakayama, T., Washizu, K., 1981. The boundary element method applied to the analysis of two dimensional nonlinear sloshing problems. *Int. J. Numer. Method Eng.*, **17**(11):1631-1646. [doi:10.1002/nme.1620171105]

Penney, W.G., Price, A.T., 1952. Finite periodic stationary gravity waves in a perfect liquid. *Phil. Trans. R. Soc. Lond. A*, **224**(882):254-284. [doi:10.1098/rsta.1952.0004]

Phillips, N.A., 1957. A coordinate system having some special advantages for numerical forecasting. *J. Meteorol.*, **14**(2):184-185. [doi:10.1175/1520-0469(1957)014<0184:ACSHSS>2.0.CO;2]

Rocca, M.L., Mele, P., Armenio, V., 1997. Variational approach to the problem of sloshing in a moving container. *J. Theoret. Appl. Fluid Mech.*, **1**(4):280-310.

Šarler, B., 2009. Solution of potential flow problems by the modified method of fundamental solutions: formulations with the single layer and the double layer fundamental solutions. *Eng. Anal. Bound. Elem.*, **33**(12):1374-1382. [doi:10.1016/j.enganabound.2009.06.008]

Tarafder, M.S., Suzuki, K., 2008. Numerical calculation of free surface potential flow around a ship using the modified Rankine source panel method. *Ocean Eng.*, **35**(5-6):536-544. [doi:10.1016/j.oceaneng.2007.11.004]

Wang, H., Zhang, H., 2007. Boundary element method for simulating the coupled motion of a fluid and a three-dimensional body. *Appl. Math. Comput.*, **190**(2):1328-1343. [doi:10.1016/j.amc.2007.02.053]

Whitham, G.B., 1965. A general approach to linear and non-linear dispersive waves using a Lagrangian. *J. Fluid Mech.*, **22**(2):273-283. [doi:10.1017/S0022112065000745]

Wu, C.H., Chen, B.F., 2009. Sloshing waves and resonance modes of fluid in a 3D tank by a time independent finite difference method. *Ocean Eng.*, **36**(6-7):500-510. [doi:10.1016/j.oceaneng.2009.01.020]

Wu, G.X., 2007. Second order resonance of sloshing in a tank. *Ocean Eng.*, **34**(17-18):2345-2349. [doi:10.1016/j.oceaneng.2007.05.004]

Zakharov, V.E., 1968. Stability of periodic waves of finite amplitude on the surface of a deep fluid. *Zh. Prokl. Mekh. Tekh. Fiz.*, **9**(2):190-194.